

# Direct Measurement of Total Vesicular Catecholamine Content with Electrochemical Microwell Arrays

Elias Ranjbari, Zahra Taleat, Mokhtar Mapar, Mohaddeseh Aref, Johan Dunevall, and Andrew Ewing\*

Cite This: *Anal. Chem.* 2020, 92, 11325–11331

Read Online

ACCESS |



Metrics &amp; More

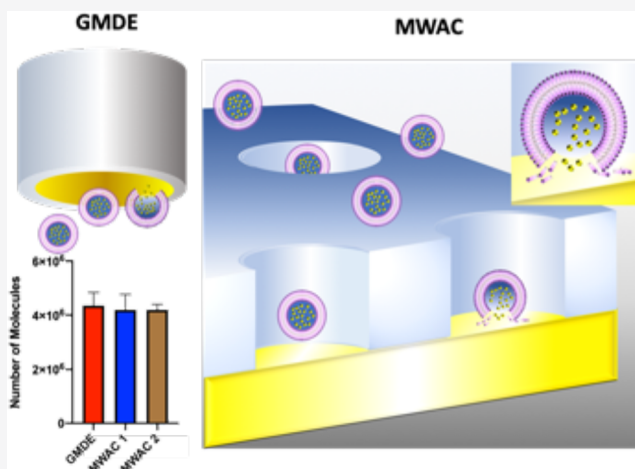


Article Recommendations



Supporting Information

**ABSTRACT:** We have designed and fabricated a microwell array chip (MWAC) to trap and detect the entire content of individual vesicles after disruption of the vesicular membrane by an applied electrical potential. To understand the mechanism of vesicle impact electrochemical cytometry (VIEC) in microwells, we simulated the rupture of the vesicles and subsequent diffusion of entrapped analytes. Two possibilities were tested: (i) the vesicle opens toward the electrode, and (ii) the vesicle opens away from the electrode. These two possibilities were simulated in the different microwells with varied depth and width. Experimental VIEC measurements of the number of molecules for each vesicle in the MWAC were compared to VIEC on a gold microdisk electrode as a control, and the quantified catecholamines between these two techniques was the same. We observed a prespike foot in a significant number of events (~20%) and argue this supports the hypothesis that the vesicles rupture toward the electrode surface with a more complex mechanism including the formation of a stable pore intermediate. This study not only confirms that in standard VIEC experiments the whole content of the vesicle is oxidized and quantified at the surface of the microdisk electrode but actively verifies that the adsorbed vesicle on the surface of the electrode forms a pore in the vicinity of the electrode rather than away from it. The fabricated MWAC promotes our ability to quantify the content of vesicles accurately, which is fundamentally important in bioanalysis of the vesicles.



Communication between neurons in the nervous system is mainly carried out through the process of exocytosis where synaptic vesicles play a crucial role.<sup>1</sup> These small and spherical organelles are responsible for loading, storing, and releasing chemical messengers, such as neurotransmitters, neurohormones, and/or neuropeptides, in cell-to-cell communication.<sup>2–9</sup> The stimulation of a neuron leads to an action potential which first causes depolarization of the membrane followed by the influx of  $\text{Ca}^{2+}$  into the cell which then triggers the exocytosis of synaptic vesicles releasing some or all of their content in the synaptic cleft. In normal brain communication, the released chemicals pass across a synaptic cleft to interact with receptors at the target cell. Bioanalysis of subcellular organelles, such as synaptic vesicles, that are required for intercellular communication is important for our perception of the mechanistic aspects of exocytosis as well as its role in synaptic plasticity.

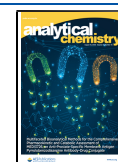
During recent years our understanding of the regulatory aspects of exocytosis has been broadened. It was previously thought that exocytosis was an all-or-none process. In this theory, after the fusion of the vesicle membrane with the cell plasma membrane, the entire content of the vesicle is expelled. It was also thought that as the initial fusion pore expanded, the

vesicular membrane fully merged with the plasma membrane of the cell, completely releasing the contents by what is often called *full fusion*. In the other hypothesis, *kiss-and-run*, it was assumed that the release of the vesicular content into the extracellular space occurs through a transient membrane fusion process.<sup>10–12</sup> In addition to kiss-and-run exocytosis, recent studies suggest that the dominant mode of what was previously thought to be full exocytosis is what might be termed *open and closed* or *partial release*.<sup>13–18</sup> Here, after fusion, the pore opens beyond that in kiss-and-run and then closes again before the full vesicle content is expelled into the extracellular compartment. On the other hand, this process is distinguished from kiss-and-run by the formation of a larger pore and the release of a larger fraction of the vesicular transmitter load. In the all-or-none mechanism, the only regulatory steps in the exocytotic

Received: May 10, 2020

Accepted: July 21, 2020

Published: July 21, 2020



process are the initiation steps (docking, priming, and fusion). In contrast, the concept of partial release with the vesicle closing again allows the cell to adjust the fusion pore size and subsequently the quantal size to control the synaptic strength.<sup>19,20</sup>

Exocytosis is a very fast process, occurring on the millisecond time-scale, and therefore techniques with high temporal resolution are needed to measure this process. Several techniques such as fluorescence microscopy have been used to investigate the exocytosis process;<sup>21,22</sup> however, due to technical limitations, temporal resolution is limited to around 20 ms. Amperometry can achieve high temporal resolution and takes advantage of the electroactivity of the catecholamines (e.g., dopamine, epinephrine, norepinephrine, serotonin, etc.), an important group of neurotransmitters and hormones. Furthermore, single cell amperometry (SCA) has been widely used to study the exocytosis process at individual cells.<sup>23,24</sup> But, to further advance the insight into the partial release process, sensitive techniques that allow measurement of the full content of individual nanometer-sized secretory vesicles had to be developed.

Vesicle impact electrochemical cytometry (VIEC), both in a flow and static format, has provided a direct measurement method for vesicular catecholamine content.<sup>15,16,25</sup> This method takes advantage of vesicle adsorption at the surface of a carbon fiber electrode in a solution containing isolated vesicles. The generation of an electrical field by the applied potential apparently causes the vesicle to rupture through electroporation, and the chemical cargo of the vesicle is oxidized at the electrode surface, giving rise to a transient current, a so-called spike.<sup>25</sup> VIEC can also be performed in situ in a living cell, without vesicle isolation, called intracellular vesicle impact electrochemical cytometry (IVIEC). Here a conical-shaped nanotip electrode is used to penetrate the cell membrane and is thus inserted into the cytoplasmic environment of the cell.<sup>17</sup> Vesicles again adsorb on the nanotip and stochastically open at the electrode surface in a potential-dependent manner.<sup>26</sup> Comparison of the catecholamines measured by EC techniques with the quantity released during exocytosis provides direct experimental evidence that in most exocytotic events a fraction of the vesicle content is released.<sup>15</sup>

An open question when using these methods to quantify the contents of vesicles is the assumption that all the catecholamines in each vesicle are captured at the electrode surface. Recently, Li et al. provided some insight into the fraction of the collected catecholamines at the underlying electrode by quantitative modeling.<sup>27</sup> They suggested that close to 100% efficiency is achieved at a 33  $\mu\text{m}$  diameter microdisk electrode in VIEC. They theoretically investigated different scenarios of PC12 cell vesicles at the surface of two different types of electrodes (disc and conical shape) and suggested that vesicle rupture occurs in close vicinity to the electrode.

In this paper, we designed a microwell-array chip-based VIEC (MWAC-VIEC) method to trap the entire content of a single vesicle and carry out accurate measurements of the vesicular cargo. Before fabrication of the MWAC, we simulated the vesicular rupture at two different positions to predict the suitable microwell dimensions (depth and width) to be confident that the entire content of the single vesicle is trapped after its rupture at the electrode surface. Bovine chromaffin cells of the adrenal medulla, with the dominant type of vesicle being a large dense core vesicle (LDCV), were used. To address the question of oxidation efficiency with

VIEC at an open microdisk electrode, the quantification results obtained by MWAC-VIEC were compared with the results at an open microdisk electrode. We show that VIEC indeed results in complete quantification of the catecholamine content of individual vesicles. Furthermore, the high frequency of prespike feet ( $\sim 20\%$ ) in the VIEC experiment is strong evidence that the rupture process includes a stable fusion-pore-like intermediate, possibly the result of the interaction between the vesicle membrane and the electrode surface.

## EXPERIMENTAL SECTION

**Chemicals and Reagents.** All chemicals were of analytical grade and obtained from Sigma-Aldrich, Sweden, unless otherwise specified. Locke's (10x) stock solution containing 1.54 M NaCl, 56 mM KCl, 36 mM NaHCO<sub>3</sub>, 56 mM glucose, and 50 mM HEPES, 1% (v/v) penicillin, adjusted at pH 7.4, was diluted 10 times with deionized water to make the working solution used for gland storage and rinsing of the adrenal vein. To provide homogenizing buffer, a solution containing 230 mM sucrose, 1 mM EDTA, 1 mM MgSO<sub>4</sub>, 10 mM HEPES, 10 mM KCl, a complete enzyme inhibitor (Roche, Sweden), DNase I (10  $\mu\text{g}/\text{mL}$ ) (Roche), and 1  $\mu\text{M}$  oligomycin was adjusted at pH 7.4. The final osmolality was checked, and it was  $310 \pm 2$  mOsm/kg. All aqueous solutions were prepared by diluting the chemicals in 18 M $\Omega$  cm<sup>-1</sup> water from a Purelab Classic purification system (ELGA, Sweden).

**Chromaffin Vesicle Isolation.** Isolation of the vesicles was performed based on the protocol adopted from the Borges group (University of La Laguna, Spain). Briefly, bovine adrenal glands were collected from the local slaughterhouse and stored in Locke's (1x) buffer solution on ice. The visible fats around the adrenal glands were removed, and the vein of each gland was rinsed three times with Locke's (1x) buffer solution or until all blood was rinsed out. Three glands were cut lengthwise, and their medulla tissue (central part) was separated from the cortex with a scalpel. Medulla tissue was homogenized in ice-cold homogenizing buffer and centrifuged at 1000g for 10 min at 4 °C to remove cell debris. The supernatant containing adrenal vesicles was transferred to another centrifuge tube to pellet them down at 10 000g for 20 min at 4 °C. The pellets were resuspended in homogenizing buffer and used as vesicle stock solution.<sup>16</sup>

**Simulations.** The openings of vesicles at different vesicle opening orientations and microwell dimensions were simulated to consider the effect of these parameters on the collection efficiency. Fick's second law (eq 1) was applied to model the transport of catecholamines from inside of the vesicle to its outside,

$$\frac{\partial c}{\partial t} = D\nabla^2 c \quad (1)$$

where  $c$  refers to the catecholamine concentration, and  $D$  is its diffusion coefficient. As the experiments were performed for vesicles isolated from chromaffin cells, the parameters used in the simulations were chosen to be representative of vesicles from these cells; the initial concentration of 600 mM catecholamine content was chosen for a vesicle with 300 nm diameter, using previously reported values for adrenal chromaffin vesicles.<sup>28</sup> In contrast, the initial concentration of catecholamine outside the vesicle was set to 0 mM. The entire surrounding boundary of the vesicle in the model was assumed to be impermeable except for a small part representing a pore (radius: 45 nm). To examine the pore formation scenarios

where the pore opens toward or away from the electrode, this pore section was assigned to the top or bottom of the simulated vesicle, respectively. The diffusion coefficient of catecholamine in the inner part of the vesicle was set as  $D_{in} = 4.1 \times 10^{-12} \text{ m}^2/\text{s}$ , which is about 2 orders of magnitude lower than that outside of the vesicle,  $D_{out} = 6.4 \times 10^{-10} \text{ m}^2/\text{s}$ .<sup>28</sup>

To carry out diffusion-limited oxidation of the catecholamine, the boundary condition at the electrode surface and boundaries representing bulk solution was set to be  $C = 0 \text{ mM}$ . Free diffusion was permitted through the pore and is described by

$$D_{out} \nabla_{out} n_{out} = -D_{in} \nabla_{in} n_{in} \quad (2)$$

where  $n$  refers to the inward pointing unit normal and the subscripts “in” and “out” represent the values of the quantities in the inner and outer domains, respectively.

Except for the pore, the other parts of the vesicle were set to be impermeable as described by

$$D \nabla c n = 0 \quad (3)$$

The equations were solved by use of COMSOL Multiphysics (version 5.2a). The selected mesh size was set to a minimum of 0.15 nm and a maximum of 1.1 nm.

The steep concentration gradient between the outside and inside of the vesicle caused a rapid decrease in the concentration of catecholamine in the vesicle. The electrode boundary condition of  $C = 0$  represented an instantaneous oxidation of catecholamine as soon as it arrived at the electrode surface, mimicking the real situation. By integrating the flux over time, the fraction of detected molecules (collection efficiency) could be simulated. Collection efficiency, defined as the total collected molecules divided by the initial number of molecules in the vesicle ( $5.1 \times 10^6$  molecules), was used as the criterion for comparing the effect of different parameters on the number of molecules encountering the electrode.

**Fabrication of Gold Microdisk Electrodes (GMDE).** To make a GMDE, a 1.0 cm piece of gold wire with a diameter of 120  $\mu\text{m}$  was soldered to a 7.0 cm long silver wire, head to head. The soldered wire was inserted in a 5 cm length of glass capillary (o.d. 1.2 mm, i.d. 0.69 mm, no filament; Sutter Instrument Co., Novato, CA), so that the Au was protruding from one end and the Ag wire from the other. The Au end was immersed into freshly made epoxy (EpoTek 301, Billerica, MA), to seal the space between gold and glass. The epoxy around the Au was cured for 8 h at room temperature and then further cured in a drying oven (110  $^{\circ}\text{C}$ ) for 1 h. The Au end of the electrode was sanded with sandpaper to expose the gold disk and eventually polished with a cloth and alumina polishing grit (0.05  $\mu\text{m}$ ).

**Design and Fabrication of the MWAC.** A 5 mm  $\times$  15 mm rectangular chip containing an array of 30  $\times$  30 microwells with the dimensions of 2.5  $\mu\text{m}$  width and 2.5  $\mu\text{m}$  depth was designed and fabricated, based on the simulation results. A 4-in. glass wafer with a thickness of 300  $\mu\text{m}$  was coated with 2 nm of chromium as an adhesion layer followed by 100 nm of gold (Figure 1) using e-beam physical vapor deposition (PVD 225, Kurt J. Lesker, Glassport, PA). The wafer was then coated with a 2.5  $\mu\text{m}$  thick layer of AZ 1512 HS photoresist by spin coating (LabSpin 6, Suss) at 1000 rpm for 30 s and soft baked at 100  $^{\circ}\text{C}$  for 1 min on a hot plate. To form the microwells on top of the gold electrode, the photoresist was exposed using a maskless direct laser writer (DWL 2000, Heidelberg Instru-

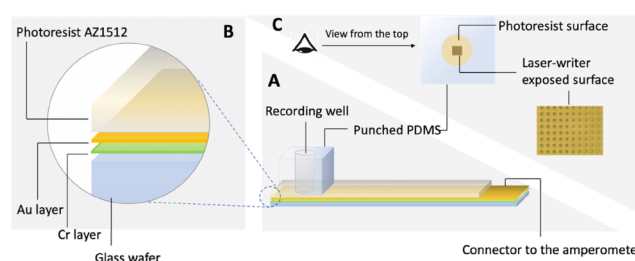


**Figure 1.** Schematic of the fabricated MWAC. (A) MWAC. (B) Zoom in to show the layer by layer of the chip. (C) Top view of the sample injection port.

ments) and developed in MF CD 26 for 1.0 min. The wafer was diced to individual chips and stored in a cleanroom environment until use. Prior to the experiment, each chip was exposed to a short and mild oxygen plasma (Batch top dry etch RIE, Plasma Therm) to make the photoresist hydrophilic and facilitate the wetting of the microwells. A PDMS block with punched holes was placed on top of the chip both to confine the vesicle suspension solution to the area with the microwells and to help immerse the reference electrode inside the solution containing vesicles (10  $\mu\text{L}$ ).

**Data Acquisition and Process.** Electrochemical measurements of vesicular content were performed using a molecular device potentiostat (model: Axopatch 200B, Molecular Devices, Sunnyvale, CA) with both MWACs and GMDEs. Both electrodes were held at 0.7 V vs an Ag/AgCl pseudoreference electrode. The output was digitized at 10 kHz using a Digidata model 1440A with Axoscope 10.3 software (Axon Instruments Inc., Sunnyvale, CA) and filtered at 2 kHz using a four-pole Bessel filter. For GMDE-VIEC, the electrode was dipped in a stock chromaffin vesicle suspension for 20 min. The electrode was then transferred to vesicle-free homogenizing buffer for the analysis. For VIEC recording with the MWAC, 10  $\mu\text{L}$  of the chromaffin vesicle suspension was added to the top of the wells through the punched PDMS block and was allowed to stand for 20 min. It was then replaced with the homogenizing buffer prior to analysis of adsorbed vesicles. The amperometric traces recorded were converted to a .txt file in MATLAB and finally processed with IgorPro 6.22 (Wavemetrics, Lake Oswego, OR). A 1-kHz binomial current filter was applied for each trace, and five times the standard deviation of the noise was used as the limitation of peak detection. The prespike transitional current, that precedes the fast upstroke of the spike and exceeds the baseline noise by two times the standard deviation, was chosen as the prespike foot. All transient spike candidates were inspected manually to reject false positive peaks.

## RESULTS AND DISCUSSION

### Simulation of Vesicle Rupture in the MWAC.

Numerical simulation of vesicular catecholamine release through the vesicle pore was performed at both vesicle opening orientations (pore opening at/close to the electrode surface or opposite the electrode surface) to compare the collection efficiency. Figure 2A and 2B simulates the opening of a vesicle at the interface with the electrode, whereas Figure 2C and 2D shows the simulation for a vesicle that forms a pore and opens opposite to the electrode surface. The pore ( $d_{pore} = 90 \text{ nm}$ ) was simulated by setting a permeable portion of the vesicle membrane to have unhindered permeability, while the remainder was impermeable. Figure S1 shows the simulated

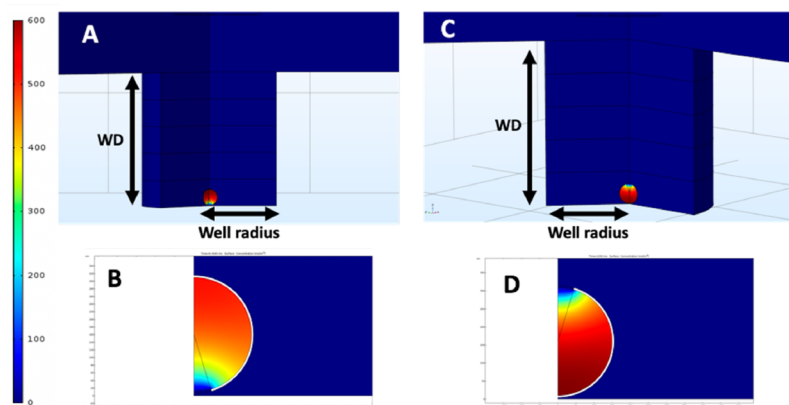


**Figure 2.** Simulation of a vesicle opening in a microwell. (A) The simulation of vesicle opening toward the electrode and the parameters that were considered (WD and WW), (B) zoomed in image in Y–Z profile for vesicle opening toward the electrode at time 4.9 ms. (C) Simulation of vesicle opening far away from the electrode. (D) Zoomed in image in Y–Z profile for vesicle opening far away from the electrode at time 5.6 ms. B and D show only half the vesicle, simulated in the 2D axisymmetric mode in COMSOL. The gradient color bar on the left side provides an estimation for the concentration of vesicle cargo during depletion. The dark red color represents 600 mM catecholamine content in the vesicle, and the dark blue represents 0 mM concentration. As the catecholamines diffuse through the pore, there is an initial concentration depression near the pore and then this depression is expanded over the vesicle in a semicircular form. The concentration profiles of the vesicular catecholamines following formation of a pore at the vesicular pole opposite and toward the electrode are shown in Supporting Information (Figure S2).

magnitude of the flux of catecholamines versus the time at the MWAC. Generally, the magnitude of the flux diminishes over time for both orientations of the vesicular pore opening. However, there is a small difference at the beginning of the plots; for the situation in which a vesicle opens toward the electrode, the decay in the flux happens immediately after running the simulation (green line), thus simulating the immediate oxidation of the catecholamines after efflux from the vesicle. In contrast, when the pore is simulated to occur on the side of the vesicle opposite to the electrode, at first the flux increases (purple line) and then it decays.

The simulation results show that when the pore is located at the bottom of vesicle that is trapped in the small well, the catecholamines are oxidized immediately at the electrode surface and 100% collection efficiency is obtained. In contrast, when the pore is on the top of the vesicle, lower collection efficiency is obtained, and it depends on the dimensions (depth and width) of the well. Figure 3 shows the plot of collection efficiency versus different well depth (WD) at five different well widths (WW). Deeper and wider wells provide higher collection efficiency. However, for microwells with dimensions larger than 2000 nm WW  $\times$  2000 nm WD, there is

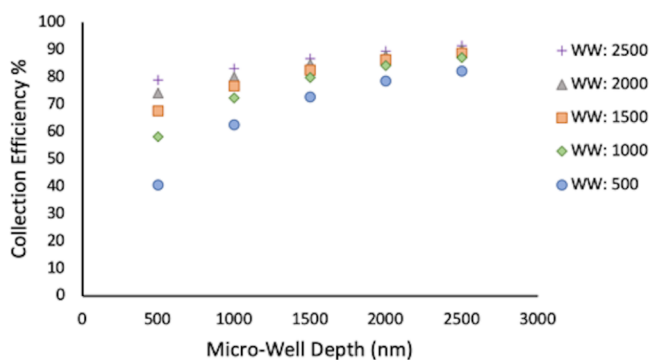


**Figure 3.** Simulated effects of depth and width of microwells on collection efficiency when the vesicle opens opposite to the electrode surface.

not a significant difference in the collection efficiency. Notably, there are significant challenges in simultaneously making deeper and narrower wells by use of the laser writer and to be able to arrive at the bottom of the well with a cylindrical shape. Furthermore, wetting the deeper wells to bring the vesicle to the bottom of the well is another challenge during the usage of these microwell arrays. Well dimensions of 2500 nm  $\times$  2000 nm (WW  $\times$  WD) were chosen as a goal for the fabrication of the microwells, and exposure to oxygen plasma greatly helps to overcome the challenge of wetting inside the wells.

**Characterization of the MWAC.** The individual holes and electrodes in the MWAC were characterized by electrochemistry, electron microscopy, and spectroscopy. To investigate the structural features of the fabricated microwell arrays, scanning electron microscopy (SEM, model: JEOL 7800F Prime) was used (Figure 4A). Elemental analysis of the bottom of the microwell was performed by energy-dispersive

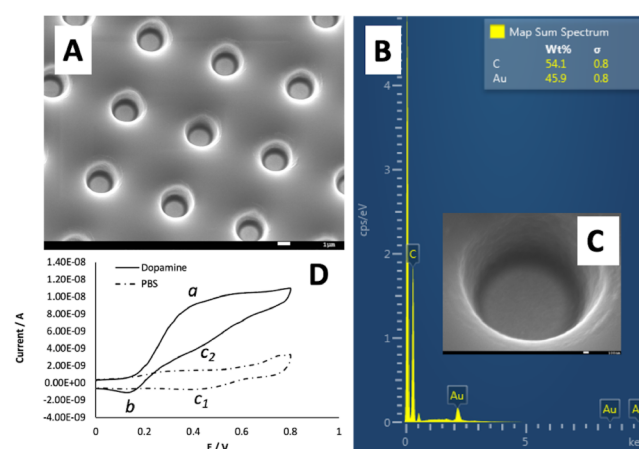


**Figure 4.** Characterization of the fabricated MWAC. (A) SEM, (B) EDX, (C) zoom in of a microwell in Figure 4A, and (D) cyclic voltammetry (scan rate of 0.1 V s<sup>-1</sup>). SEM images were acquired while operating at 5.0 kV acceleration voltage and 10 mm work distance.

X-ray spectrometry (EDX). Figure 4B shows the elemental characteristics of the area shown in Figure 4C of the EDX spectrum. These data show that laser writing lithography successfully removes the photoresist layer to reveal the gold electrode surface at predetermined spots. Microwell depths were also investigated by atomic force microscopy (AFM) as shown in Figure S3. Figure 4D shows cyclic voltammetry for a 100  $\mu\text{M}$  dopamine solution (solid line) and buffer (PBS) solution in the voltage range of 0.0–0.8 V on a microwell array chip. Dopamine is oxidized to dopamine *o*-quinone (peak a) when scanning from 0.0 to 0.8 V and back (peak b). A very weak reduction peak (peaks  $c_1$  and  $c_2$  in the respective voltammograms) in both the blank and dopamine solutions is observed. These latter peaks are related to the reduction of the gold oxide layer;<sup>29</sup> as we use 0.7 V potential for VIEC, these peaks do not interfere in our measurements. Generally, the fabricated chip provides a substrate with good reaction kinetics and stable steady-state current for dopamine oxidation, thus indicating it should be suitable for vesicle analysis with VIEC.

**Comparison of VIEC in the MWAC versus an Open Electrode.** The catecholamine content of vesicles was investigated to compare VIEC at a MWAC to VIEC at an open electrode, GMDE. We have previously shown that the vesicles rupture stochastically in VIEC, with the rupturing probability having a strong dependence on applied potential.<sup>26</sup> Not all vesicles rupture, however, and it is still difficult to precisely define this number. The catecholamines arrive at the electrode surface, giving rise to a typical transient current (a spike) as observed in Figure 5A and 5B, for VIEC with the

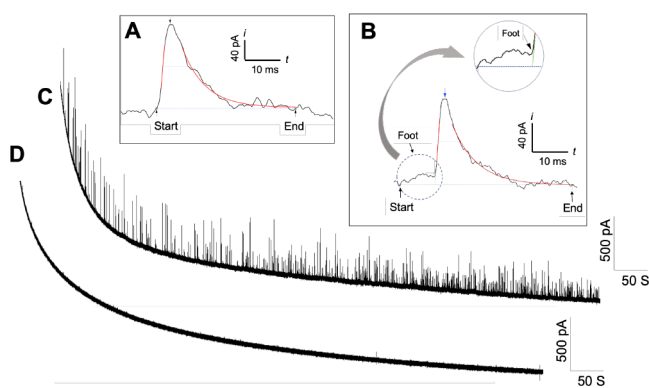


**Figure 5.** Representative transient amperometric spikes (A) without a prespike foot and (B) with a prespike foot for a single vesicle at the MWAC. Representative amperometric traces of (C) VIEC with MWAC and (D) background signal at a MWAC. Traces for oxidation current were recorded at +0.7 V with respect to Ag/AgCl pseudoreference electrode.

MWAC. The number of molecules in each individual vesicle,  $N$ , during VIEC at the electrode surface can be calculated by Faraday's law (eq 4):

$$N = \frac{Q}{nF} \quad (4)$$

where  $n$  is the number of electrons in the oxidation reaction (2 electrons for catecholamines),  $F$  is the Faraday constant (96 485 C mol<sup>-1</sup> of electrons), and  $Q$  is the charge calculated by integrating current for each amperometric spike. Applying potential to the vesicle-preloaded MWAC leads to a sequence of vesicle ruptures at the electrode surface that provide an amperometric trace of transient currents (spikes), which is

shown in Figure 5C. No spikes are observed when the MWAC is loaded by a homogenizing buffer lacking vesicles (Figure 5D). Typical traces obtained at the GMDE are shown in Figure S4.

Multiple mechanisms have been proposed for the opening of the vesicle and release at the electrode surface including catecholamine release through collapse of the vesicle at the electrode surface or during formation of a pore in the vesicle at the interface of the vesicle and the electrode.<sup>27</sup> Cheng et al. investigated oxidation of vitamin C-encapsulated liposomes at a carbon electrode surface and proposed that the liposome immediately collapses and releases its entire cargo as “full-collapse fusion”.<sup>30</sup> Li et al. simulated bursting of the vesicle at microdisk and nanotip electrodes; they concluded that the opening mechanism of mammalian vesicles, unlike the liposomes, proceeds via “pore formation” at the electrode surface.<sup>27</sup> In the work presented here, we found that 21% of the spikes in whole traces of MWAC-VIEC and 23% of the total spikes in the traces of GMDE-VIEC are accompanied by a prespike foot thought to result from a small pore that opens in the vesicle membrane at the electrode prior to the pore dilating and subsequent full electrolysis of the vesicle contents.

Although all aspects of the mechanism of the vesicle rupture in VIEC are not clear yet, observations of the prespike foot in the VIEC provides some clues to gain insight into the perception of the vesicle rupture at the electrode surface. As previously described by Lovric et al.,<sup>26</sup> the vesicle membrane is decorated with proteins that form a barrier to the membrane phospholipids contacting the electrode. As these stochastically move, they can allow close contact and electroporation. This hypothesis could be related to observing the prespike foot in VIEC, as in some cases the vesicle surface area for pore formation can be limited by these vesicle membrane proteins. The observation of the prespike foot in VIEC argues for the electroporation mechanism of vesicle rupture at the electrode surface; the phenomenon is similar but distinct from what is observed during the exocytosis events in live cells. In VIEC the pore opens from the vesicle to the electrode, whereas in exocytosis it is caused by the two fusing membranes. In both cases the pore seems to be regulated and static for a short time, probably mediated by proteins.

The observation of the prespike foot in this work is in agreement with the results reported by Li et al.<sup>31</sup> and appears to confirm that vesicle rupture at the electrode surface is much more complex than a simple collapse mechanism. This observation promotes the hypothesis that the vesicular rupture occurs via an electroporation mechanism through the formation of a stable pore intermediate.<sup>26</sup>

The distribution of the mole amount of catecholamines for a series of individual current transients in GMDE-VIEC and MWAC-VIEC is shown as a normalized frequency histogram of vesicle content in Figure 6A. These distributions show a similar trend. Also, when directly comparing the number of molecules measured by MWAC-VIEC to that obtained by GMDE-VIEC (Figure 6B), no significant difference is observed (Wilcoxon–Mann–Whitney test). Thus, whether the vesicle opens toward the electrode or at the vesicular pole opposite the electrode, on the GMDE, VIEC measures the entire vesicular content. To determine whether the vesicles open at the pole close to the electrode, we performed VIEC with microwells having two different dimensions, one with 2.5- $\mu\text{m}$  WW  $\times$  2.0- $\mu\text{m}$  WD dimension (MWAC1) and the other with 1.5- $\mu\text{m}$  WW  $\times$  0.5- $\mu\text{m}$  WD dimension (MWAC2). The

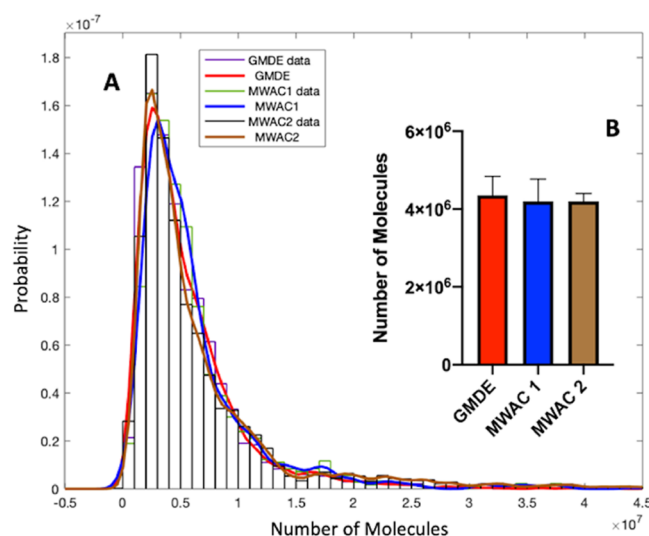


**Figure 6.** Number of molecules from chromaffin vesicles measured by GMDE-VIEC and MWAC-VIEC. (A) Histograms of the distribution of the number of molecules, results from GMDE-VIEC (red line) and MWAC-VIEC (MWAC1 (blue line): microwell with 2.5- $\mu\text{m}$  WW  $\times$  2.0- $\mu\text{m}$  WD dimensions; MWAC2 (brown line): microwell with 1.5- $\mu\text{m}$  WW  $\times$  0.5- $\mu\text{m}$  WD dimensions). (B) Bar plots of the number of molecules obtained by GMDE-VIEC (red) and MWAC-VIEC (MWAC1 (blue): microwell with 2.5- $\mu\text{m}$  WW  $\times$  2.0- $\mu\text{m}$  WD dimensions; MWAC2 (brown): microwell with 1.5- $\mu\text{m}$  WW  $\times$  0.5- $\mu\text{m}$  WD dimensions). The error bars are the standard error of mean (SEM).

simulated results for VIEC in these wells (Figure 3) showed an expected lower collection efficiency for MWAC2, with smaller dimensions, when compared to MWAC1 when the vesicles open at the pole 180° away from the electrode. However, the experimental results show that comparing VIEC in smaller versus larger microwells does not have a significant effect on the number of molecules measured. This suggests that the collection efficiency for both sizes of microwells are the same. Thus, we conclude that vesicles undergoing VIEC open at the pole close to the electrode and not to the opposite pole.

## CONCLUSIONS

The work reported here presents the development of a new kind of VIEC technique based on a MWAC to successfully gain further insights into the mechanism of vesicle rupture at the surface of an electrode. The MWAC approach allows physical trapping of the entire content of a single vesicle after it ruptures in the base of a microwell, which leads to complete electrochemical detection of its content. This cannot be performed with normal disk-shaped electrodes. Before fabrication of the MWAC, simulation of a ruptured single vesicle at the bottom of the microwell showed that when the vesicle pore is located toward the electrode the collection efficiency is 100% and it is independent of the dimensions of the microwell whereas collection efficiency is dimension dependent if the vesicle pore is formed far away from the electrode and the maximum efficiencies are obtained at microwell dimensions larger than 2  $\mu\text{m}$ . A comparison of the number of molecules measured by MWAC-VIEC showed excellent agreement with the GMDE-VIEC results. It also confirms that in conventional VIEC experiments utilizing disk-shaped electrodes, close to 100% collection efficiency is obtained. Moreover, changes in the dimensions of the

microwells do not have any significant effect on the experimental results obtained by the VIEC. This confirms the hypothesis that the vesicles open at the pole close to the electrode. Furthermore, the presence of a prespike foot in  $\sim 20\%$  of events supports the hypothesis that the vesicles rupture toward the electrode surface with a more complex mechanism including the formation of a stable pore intermediate prior to the vesicle opening all the way.

## ASSOCIATED CONTENT

### Supporting Information

The Supporting Information is available free of charge at <https://pubs.acs.org/doi/10.1021/acs.analchem.0c02010>.

Simulated magnitude of the flux versus the time, the concentration profiles of the vesicular catecholamines following formation of a pore at the vesicular pole opposite and toward the electrode, atomic force microscopy (AFM) of the microwell array chip (MWAC), and representative vesicle impact electrochemical cytometry (VIEC) traces recorded for chromaffin cell vesicles at a gold microdisk electrode (GMDE) (PDF)

## AUTHOR INFORMATION

### Corresponding Author

Andrew Ewing – Department of Chemistry and Molecular Biology, University of Gothenburg, Gothenburg, Sweden; [orcid.org/0000-0002-2084-0133](https://orcid.org/0000-0002-2084-0133); Email: [andrew@chem.gu.se](mailto:andrew@chem.gu.se)

### Authors

Elias Ranjbari – Department of Chemistry and Molecular Biology, University of Gothenburg, Gothenburg, Sweden  
 Zahra Taleat – Department of Chemistry and Molecular Biology, University of Gothenburg, Gothenburg, Sweden  
 Mokhtar Mapar – Division of Biological Physics, Department of Applied Physics, Chalmers University of Technology, SE-41296 Gothenburg, Sweden  
 Mohaddeseh Aref – Department of Chemistry and Molecular Biology, University of Gothenburg, Gothenburg, Sweden  
 Johan Dunevall – Department of Chemistry and Molecular Biology, University of Gothenburg, Gothenburg, Sweden; [orcid.org/0000-0001-9188-9893](https://orcid.org/0000-0001-9188-9893)

Complete contact information is available at: <https://pubs.acs.org/doi/10.1021/acs.analchem.0c02010>

### Author Contributions

All authors have given approval to the final version of the manuscript.

### Notes

The authors declare no competing financial interest.

## ACKNOWLEDGMENTS

The authors acknowledge funding from the European Research Council (ERC), Knut and Alice Wallenberg Foundation, Swedish Research Council (VR), and the National Institutes of Health. E.R. acknowledges funding from the Human Frontier Science Program Organization (HFSPO; reference number: LT 000407/2017C). M.A. acknowledges funding from the European Union's Horizon 2020 research and innovation program under the Marie Skłodowska-Curie grant agreement no. 793324. We thank Dalsjöfors Kött AB, Sweden, and their

employees for their kind help with providing the adrenal glands.

## REFERENCES

- (1) Jahn, R.; Sudhof, T. C. *Annu. Rev. Neurosci.* **1994**, *17* (1), 219–246.
- (2) He, L.; Xue, L.; Xu, J.; McNeil, B. D.; Bai, L.; Melicoff, E.; Adachi, R.; Wu, L.-G. *Nature* **2009**, *459* (7243), 93.
- (3) Jahn, R.; Fasshauer, D. *Nature* **2012**, *490* (7419), 201.
- (4) Mohrmann, R.; De Wit, H.; Verhage, M.; Neher, E.; Sørensen, J. B. *Science* **2010**, *330* (6003), 502–505.
- (5) Watanabe, S. *Science* **2015**, *350* (6256), 46–47.
- (6) Majdi, S.; Berglund, E. C.; Dunevall, J.; Oleinick, A. I.; Amatore, C.; Krantz, D. E.; Ewing, A. G. *Angew. Chem.* **2015**, *127* (46), 13813–13816.
- (7) Li, Y. T.; Zhang, S. H.; Wang, X. Y.; Zhang, X. W.; Oleinick, A. I.; Svir, I.; Amatore, C.; Huang, W. H. *Angew. Chem., Int. Ed.* **2015**, *54* (32), 9313–9318.
- (8) Lemaitre, F.; Guille Collignon, M. G.; Amatore, C. *Electrochim. Acta* **2014**, *140*, 457–466.
- (9) Amatore, C.; Delacotte, J.; Guille-Collignon, M.; Lemaitre, F. *Analyst* **2015**, *140* (11), 3687–3695.
- (10) Elhamdani, A.; Azizi, F.; Artalejo, C. R. *J. Neurosci.* **2006**, *26* (11), 3030–3036.
- (11) Wightman, R. M.; Haynes, C. L. *Nat. Neurosci.* **2004**, *7* (4), 321.
- (12) Wang, C.-T.; Lu, J.-C.; Bai, J.; Chang, P. Y.; Martin, T. F.; Chapman, E. R.; Jackson, M. B. *Nature* **2003**, *424* (6951), 943.
- (13) Omiatek, D. M.; Dong, Y.; Heien, M. L.; Ewing, A. G. *ACS Chem. Neurosci.* **2010**, *1* (3), 234–245.
- (14) Amatore, C.; Oleinick, A. I.; Svir, I. *ChemPhysChem* **2010**, *11* (1), 159–174.
- (15) Ren, L.; Mellander, L. J.; Keighron, J.; Cans, A.-S.; Kurczy, M. E.; Svir, I.; Oleinick, A.; Amatore, C.; Ewing, A. G. The evidence for open and closed exocytosis as the primary release mechanism. *Q. Rev. Biophys.* **2016**, *49*. DOI: 10.1017/S0033583516000081
- (16) Dunevall, J.; Fathali, H.; Najafinobar, N.; Lovric, J.; Wigström, J.; Cans, A.-S.; Ewing, A. G. *J. Am. Chem. Soc.* **2015**, *137* (13), 4344–4346.
- (17) Li, X.; Majdi, S.; Dunevall, J.; Fathali, H.; Ewing, A. G. *Angew. Chem., Int. Ed.* **2015**, *54* (41), 11978–11982.
- (18) Ranjbari, E.; Majdi, S.; Ewing, A. *Trends Chem.* **2019**, *1* (4), 440–451.
- (19) Zhu, W.; Gu, C.; Dunevall, J.; Ren, L.; Zhou, X.; Ewing, A. G. *Angew. Chem., Int. Ed.* **2019**, *58* (13), 4238–4242.
- (20) Gu, C.; Larsson, A.; Ewing, A. G. *Proc. Natl. Acad. Sci. U. S. A.* **2019**, *116* (43), 21409–21415.
- (21) Zhao, W.-D.; Hamid, E.; Shin, W.; Wen, P. J.; Krystofiak, E. S.; Villarreal, S. A.; Chiang, H.-C.; Kachar, B.; Wu, L.-G. *Nature* **2016**, *534* (7608), 548.
- (22) Mattila, J.-P.; Shnyrova, A. V.; Sundborger, A. C.; Hortelano, E. R.; Fuhrmans, M.; Neumann, S.; Müller, M.; Hinshaw, J. E.; Schmid, S. L.; Frolov, V. A. *Nature* **2015**, *524* (7563), 109.
- (23) Wightman, R.; Jankowski, J.; Kennedy, R.; Kawagoe, K.; Schroeder, T.; Leszczyszyn, D.; Near, J.; Diliberto, E.; Viveros, O. *Proc. Natl. Acad. Sci. U. S. A.* **1991**, *88* (23), 10754–10758.
- (24) Oomen, P. E.; Aref, M. A.; Kaya, I.; Phan, N. T. N.; Ewing, A. G. *Anal. Chem.* **2019**, *91* (1), 588–621.
- (25) Omiatek, D. M.; Santillo, M. F.; Heien, M. L.; Ewing, A. G. *Anal. Chem.* **2009**, *81* (6), 2294–2302.
- (26) Lovrić, J.; Najafinobar, N.; Dunevall, J.; Majdi, S.; Svir, I.; Oleinick, A.; Amatore, C.; Ewing, A. G. *Faraday Discuss.* **2016**, *193*, 65–79.
- (27) Li, X.; Ren, L.; Dunevall, J.; Ye, D.; White, H. S.; Edwards, M. A.; Ewing, A. G. *ACS Nano* **2018**, *12* (3), 3010–3019.
- (28) Amatore, C.; Bouret, Y.; Midrier, L. *Chem. - Eur. J.* **1999**, *5* (7), 2151–2162.
- (29) Dudin, P. V.; Unwin, P. R.; Macpherson, J. V. *Phys. Chem. Chem. Phys.* **2011**, *13* (38), 17146–17152.
- (30) Cheng, W.; Compton, R. G. *Angew. Chem., Int. Ed.* **2014**, *53* (50), 13928–13930.
- (31) Li, X.; Dunevall, J.; Ren, L.; Ewing, A. G. *Anal. Chem.* **2017**, *89* (17), 9416–9423.